Hydrosedimentological Response to Estuarine Deepening
Conceptual Analysis

Winterwerp, Johan C.; Wang, Zheng-Bing

DOI
10.1061/(ASCE)WW.1943-5460.0000660

Publication date
2021

Document Version
Accepted author manuscript

Published in
Journal of Waterway, Port, Coastal and Ocean Engineering

Citation (APA)
Winterwerp, J. C., & Wang, Z.-B. (2021). Hydrosedimentological Response to Estuarine Deepening: Conceptual Analysis. *Journal of Waterway, Port, Coastal and Ocean Engineering*, *147*(5), 04021023-1 - 04021023-10. Article 04021023. https://doi.org/10.1061/(ASCE)WW.1943-5460.0000660

Hydro-sedimentological response to estuarine deepening – a conceptual analysis

by Johan C. Winterwerp[1)] and Zheng-Bing Wang[2)]

1) Professor, Delft University of Technology, Faculty of Civil Engineering and Geosciences, Department of Coastal Engineering, Section of Environmental Hydraulics, Stevinweg 1, 2628CN, Delft, The Netherlands, email: j.c.winterwerp@tudelft.nl
2) Senior Specialist, Deltares, Boussinesqweg 1, 2629 HV Delft, The Netherlands, email: zeng.wang@deltares.nl, also: Professor, Delft University of Technology, Faculty of Civil Engineering and Geosciences, Department of Coastal Engineering, Section of Hydraulic Engineering, Stevinweg 1, 2628CN, Delft, The Netherlands.

Abstract

This paper describes the effects of anthropogenic deepening of tidal rivers in a conceptual way, with focus on tidal distortion and the residual transport of coarse sediment, driven by asymmetries in peak velocity. The rivers under consideration are fairly small, with small river discharge, and may have irregular hypsometry, with substantial intertidal area, or not. Residual sediment transport is driven by asymmetries in tidal velocity (horizontal tide), which is however difficult to establish in general. This paper discusses how and under which cases asymmetries in tidal elevations (vertical tide) can provide appropriate information on residual sediment transport. It is argued that deepening may induce a competition between an increase in tidal amplitude by amplification and a reduction in the asymmetry itself. Linear analysis shows that tidal asymmetry may show irregular behavior locally even for regular river configurations. It is therefore expected that these irregularities become larger in natural and engineered rivers. Analysis of local asymmetries may therefore misleading in assessing the river's response to deepening with respect to the overall residual sediment transport, and the river's morphology.

Thus analysis of the overall morphodynamic response of a tidal river to tidal asymmetry, as affected by deepening requires integration of the non-linear effects along the entire river. It is argued that tidal asymmetry can be quantified by determining the difference in travel times of the high and low waters at any location within the river. This also implies that tidal water level variations and their asymmetries are governed by the entire tidal volume up-river of the cross section under consideration. River discharge further complicates the analyses by affecting residual water flows, effective hydraulic drag, tidal asymmetry and mean water level. These effects reduce in response to deepening. However, salinity intrusion and gravitational circulation increase with deepening. We believe that assessing the (long-term) effects of deepening a fairway in a tidal river or estuary requires the use of process-based numerical models to account for all these non-linear interactions, next to appropriate data collection. The current paper may help analyzing and interpreting the numerical results.

Key words: tidal river, deepening, tidal asymmetry, residual sediment transport

Introduction

To accommodate for the ongoing growth in size of seagoing vessels, fairways in estuaries and tidal rivers are deepened and widened frequently. The offset from their equilibrium morphology generally requires maintenance of the deepened fairways, e.g. in the form of maintenance dredging. The volumes of maintenance dredging have always been a major concern to the managing authorities, as these could contribute substantially to the operational costs of a port. Today, authorities are concerned also with the autonomous response of estuaries and tidal rivers to deepening, as such interventions may induce another morphodynamic equilibrium, with unfavorable changes in the local ecosystem. Two examples of such unfavorable autonomous response to narrowing and deepening are the Elbe and Loire Rivers (Winterwerp et al, 2013b), which evolved to hyper-turbid conditions with significant water quality problems. Another example is the deepening of the Western Scheldt estuary due to sand mining and excavation of parts of the estuaries thalweg to accommodate for larger ships (Wang et al., 2015) This deepening reduced sediment import from the North Sea and induced larger tidal flow velocities in the channels which in turn led to accretion thus heightening of the tidal flats, losing valuable ecosystem habitat (Wang et al., 2015; De Vet et al., 2017). In all cases, this autonomous behavior is steered by changes in residual sediment transport in response to anthropogenic interventions/deepening in the aquatic system, induced by:

1. changes in baroclinic effects: the near-bed residual flow induced by gravitational circulation scale with the cube of the water depth, hence increases considerably with deepening, and
2. changes in barotropic effects: tidal amplification, tidal asymmetry and the effects of river flow are modified in response to deepening of a tidal river.

The present paper focuses on the effects of anthropogenic deepening on tidal amplification and tidal asymmetry in narrow tidal rivers, characterized by a single tidal channel. Its thalweg generally defines the fairway, and excavation of the thalweg for navigational purposes therefore generally implies deepening of the river.

In general, residual sediment transport is steered by asymmetries in hydrodynamic forcing and/or in sedimentological processes and properties. The response of fine (cohesive) sediment to such asymmetries is controlled by its limited availability and profound time lag effects (Winterwerp et al., 2021), while residual transport of sandy sediments is generally steered by asymmetries in peak velocity., The response of coarse and fine sediment to fairway deepening is therefore rather different, both qualitatively and quantitatively. In this paper we focus on the residual transport of coarse sediment by tidal asymmetry, the transport of which follows equilibrium relations with small time lag effects. We ignore other asymmetry effects such as those in bathymetry (Jeuken and Wang, 2010) and those induced by the management of the river, such as dredging and dumping activities (Wang et al., 2015). Hence, the discussions in this paper are relevant for narrow sandy estuary and tidal rivers, ignoring the salt-fresh water induced gravitational circulation.

Tidal asymmetry is generally explained from the first harmonic overtide M4 of the semi-diurnal M2 tide (see e.g. Friedrichs and Aubrey, 1988):

$$u(t) = u_2 \cos(\omega t - \phi_2) + u_4 \cos(2\omega t - \phi_4) \quad (1)$$

where u_2 and u_4 represent the tidal velocity amplitude induced by the M2 and M4 tide, with their phase angles ϕ_2 and ϕ_4. The double frequency of M4 tide stems for instance from non-linear advection (*uu*) and friction $\left(u|u|/h\right)$ terms in the momentum equation (Parker, 1991; Provost, 1991). We elaborate on the formation of the overtides (higher harmonics) further below. It can be shown that for relative phase differences $-90^{\circ} < 2\phi_2 - \phi_4 < 90^{\circ}$, peak flood velocities (defined as positive here) exceed their ebb values. As sediment transport T scales non-linearly with velocity $\left(T \propto u^n \text{ with } n > 3\right)$, this would imply flood-dominant residual sediment transport. Deepening of a fairway reduces the tidal deformation, i.e. the asymmetry becomes smaller – *in extremo*, tidal asymmetry is absent, as in oceans. However, deepening may also increase the tidal velocity amplitude through amplification and/or reduction in friction-induced damping. Hence, the ultimate residual sediment transport response to deepening is governed by a competition between tidal deformation and tidal amplification.

Unfortunately, asymmetries in flow velocity are often difficult to assess. In the case of field data, velocity time series are generally not complete. In the case of mathematical models, interpretation problems may arise if flow velocities change in direction over time (tidal ellipses), or are not equally distributed over the cross section (bends). Therefore, tidal asymmetry is often analyzed on the basis of water levels. In the following, asymmetries in tidal flow velocity are referred to as asymmetry in the horizontal tide, and similarly, asymmetries in tidal elevations are referred to as asymmetries inn the vertical tide. Of course, both are closely related because of continuity, as shown below.

In the next section, some concepts in the literature on residual sediment transport by tidal asymmetry is summarized, showing when these concepts converge, including the role of the hypsometry (shape of the cross section) on the flood-ebb-dominance transition. Next, the role of the competition between tidal deformation and amplification on residual transports in response to deepening is investigated with a linear approach. Then the morphodynamic response of a tidal river to deepening is discussed in a conceptual way, including the role of "external asymmetry", i.e. tidal asymmetry generated beyond the boundaries of the tidal river under consideration, and the role of river flow. It is argued that analysis of tidal asymmetry at a single station may be misleading in analyzing residual transport in a tidal river at river scale.

Tidal asymmetry and local residual sediment transport

Though literature contains multiple publications on tidal asymmetry and residual sediment transport, we focus on the work by Friedrichs and Aubrey (1988) and Dronkers (1986), as their concepts form the basis of basically all subsequent publications. Both concepts analyze tidal deformation in the prismatic channel of Fig. 1 with a flow-carrying cross section with area V_c and width at low water (LW) b_c, and an intertidal cross section with total area V_s, which only stores water, i.e. flow velocities are assumed zero. The total width at high water (HW) measures b_{tot}.

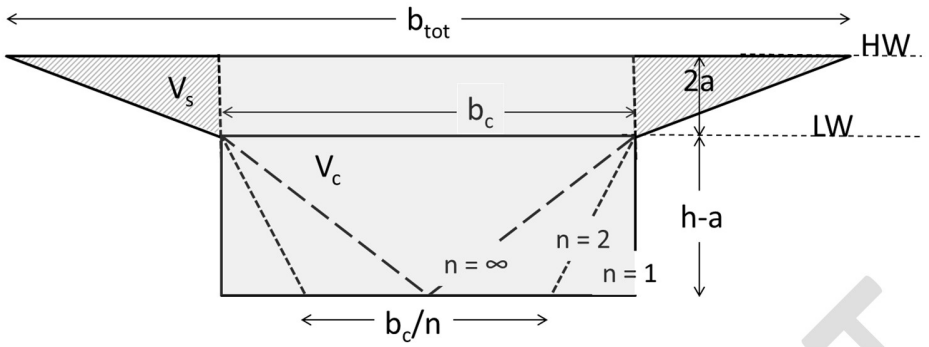

Fig. 1: Schematic of estuary hypsometry of Speer and Aubrey (1985) and Wang et al. (2002) with storage (intertidal) area V_s and flow-carrying cross section V_c, and definition of shape parameter n.

Speer and Aubrey (1985) presented a numerical solution for a 7 km long, semi-enclosed tidal basin with a cross-section represented by n =2 in Fig. 1. This study was extended by Friedrichs and Aubrey (1988), using the same configuration, prescribing an M2 tide with 0.75 m amplitude at the model boundary and a constant friction coefficient f = 0.01 $\left(\tau_b = \rho f U^2\right)$. They carried out 84 numerical simulations, varying water depth h and intertidal area V_s, while keeping $b_c = 120h$. The results of these simulations were analyzed in terms of the sea level distortions induced within the basin at four locations (1.5; 3.3; 5.0; and 6.8 km from mouth) as visualized in the diagram of Fig. 2, showing the M4/M2 amplitude ratio and phase difference $2\phi_2 - \phi_4$ as a function of relative tidal range (tidal amplitude to depth ratio) and relative intertidal area (the ratio between tidal storage volume above intertidal flat and channel volume). The transition between flood- and ebb-dominant is reflected by the co-phase line of 180° (Fig. 2, right panel). Note that because of the very short basin (with respect to the tidal wave length) considered, horizontal and vertical tide are 90° out of phase. Hence the 180° co-phase line for sea level distortion corresponds to a 90° transition phase angle for the horizontal tide, as in equ. (1). Note that in the long, sandy tidal rivers subject of the present study, the vertical tide lags only a few hours behind the horizontal tide. From linear theory a phase angle of 45° is found for infinitely long channels with large bed roughness and exponentially converging planform (see below)

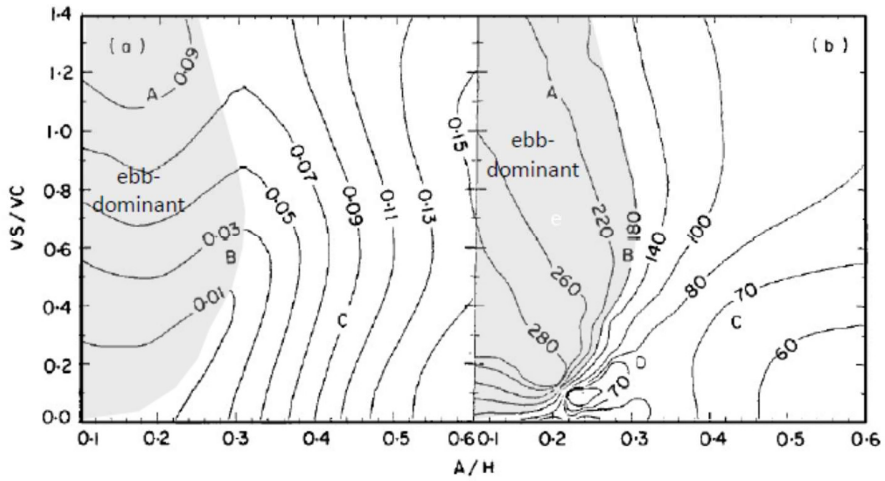

Fig. 2: Ebb-flood dominance transition diagram by Friedrichs and Aubrey (1988) for a 7 km long tidal basin and Fig. 1 cross section with n = 2.

While the analysis by Friedrichs and Aubrey (1988) on asymmetry of the vertical tide is based on the numerical solution of a full non-linear model, Dronkers (1986) analyzed the asymmetry in the horizontal tide, i.e. in the tidal velocity using a weakly non-linear approach based on an analytical solution of the propagation of a tidal wave. This allows for a more general tidal river configuration. He showed that the difference between the flood and ebb duration in the mouth of a tidal basin, $\Delta t_{fl} - \Delta t_{ebb}$ can be related to the morphology of the basin. For basins with the cross-sections of Fig.1 he found:

$$\Delta t_{fl} - \Delta t_{ebb} \propto (h-a)\frac{V_{c,LW}}{b_c} - (h+a)\frac{V_{c,HW}}{b_{tot}} \tag{2}$$

where h is mean water depth, $V_{c,LW}$ and $V_{c,HW}$ are the flow-carrying cross-sectional area at low and high water, respectively, and the other parameters are defined in Fig. 1. The transition between ebb- and flood-dominant residual sediment transport occurs when $\Delta t_{fl} = \Delta t_{ebb}$.

Wang et al. (1999) showed that the results from these two seemingly different approaches are similar by applying the relation by Dronkers to the basin considered by Friedrichs and Aubrery (1988), see Fig. 3 in comparison to Fig.2. A generalization of Dronkers' analysis for arbitrary cross sections (i.e. all values of n in Fig. 1) gives the transition between ebb- and flood-dominant residual transport (see also Wang et al. (1999):

$$\frac{V_s}{V_c} = \frac{\left(\frac{4n}{n+1}\right)\left(\frac{a}{h}\right)^2 \Big/ \left(1-\frac{a}{h}\right)}{\left(\frac{n+1}{2n}\right)+\left(\frac{n-1}{2n}\right)\frac{a}{h}} \tag{3}$$

This relation is visualized in Fig. 3a, for three values of n, i.e. a rectangular channel (n = 1), the configuration by Speer and Aubrey (n = 2), and a triangular flow-carrying cross section ($n = \infty$). Also the relation by Dronkers (1986) is given, showing qualitative agreement. For small a/h and V_s/V_c, Fig.3a is

very similar to the results by Friedrichs and Aubrey (1986). Moreover, Fig. 3a shows that not only the intertidal area and relative tidal range are important, but that this transition is also largely affected by the hypsometry of the tidal river/basin. This implies that flood- and ebb-dominant conditions may alternate locally along a tidal river.

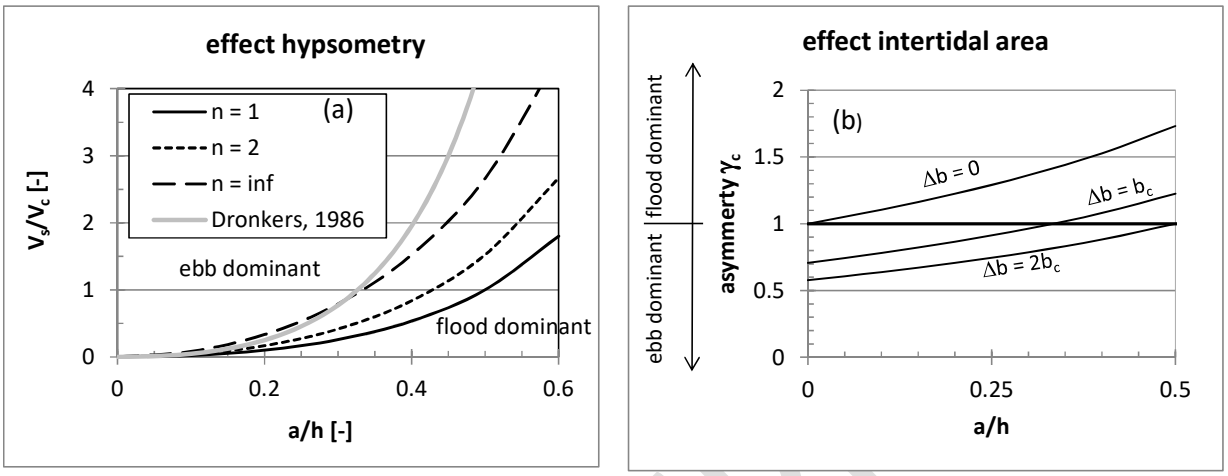

Fig. 3: (a): Ebb-flood dominance transition diagram according to Wang et al. (1999) and Dronkers (1986) as a function of hypsometry, and (b) effect intertidal area on transition for n = 1.

Further, Wang et al. (1999) demonstrate that the most important physical mechanism for tidal deformation can be parameterized throughthe tidal propagation velocity (celerity) as a function of the water level. Thus the transition from flood- to ebb-dominant conditions can also be approximated by requiring that celerities at HW and LW are identical. Dronkers (2005) used this argument by introducing the asymmetry parameter γ_c, reflecting the ratio of the tidal wave celerity at high water and low water. Flood-dominant residual transport would then be met when $\gamma_c > 1$:

$$\gamma_c = \frac{c_{\mathrm{HW}}}{c_{\mathrm{LW}}} = \frac{\sqrt{gV_{c,\mathrm{HW}}/\left(V_{s,\mathrm{LW}}\right)}}{\sqrt{gV_{c,\mathrm{LW}}}} \text{ for } n=1 \Rightarrow \gamma_c = \frac{\sqrt{g\left(h+a\right)b_c/\left(b_c+\Delta b\right)}}{\sqrt{g\left(h-a\right)}} = \sqrt{\frac{\left(1+a/h\right)b_c}{\left(1-a/h\right)\left(b_c+\Delta b\right)}} \quad (4)$$

where Δb is the width of the intertidal area. Relation (4) is elaborated for n =1, and plotted in Fig. 3b, showing that for small intertidal area, deepening of the tidal river may change the asymmetry from ebb- to flood dominant conditions, at small intertidal area. This implies that the possible amplification of the tide in response to deepening has to be accounted for.

Tidal amplification and asymmetry and local residual sediment transport

In the following, we study tidal amplification and asymmetry of a tidal wave in a tidal river with the prismatic cross section of Fig. 4, assuming a horizontal river bed and an exponentially converging width, given by $b_c = b_0 \exp\{-x/L_b\}$, where b_c is the width of the rivers flow-carrying cross section with b_0 at its mouth, and L_b is the convergence length (typical values between ~20 and ~40 km). Furthermore, we

assume a rectangular shape of the flow-carrying cross section, such that $V_c \approx hb_c$ The width of the intertidal area, denoted by Δb, is a constant fraction of $b_c(x)$; hence Δb is also an exponential function of x. We introduce the complex wave number k, which consists of a real part k_r and an imaginary part k_i, representing wave length and wave dissipation, respectively. Thus $k = k_r + ik_i$. Appendix A describes the derivation of the equations for relative tidal amplification and asymmetry:

$$\frac{a(x)}{h} = \frac{a_0}{h}\frac{a}{a_0} = \frac{a_0}{h}\exp\left\{\frac{1}{2L_b}\left(1-\frac{1}{2}\left[2\sqrt{\left(\Lambda_e-1\right)^2+\left(\Lambda_e r_*\right)^2}-2\left(\Lambda_e-1\right)\right]^{1/2}\right)x\right\} \tag{5}$$

and for the asymmetry parameter γ_c:

$$\gamma_c(x) = \frac{k_{r,LW}}{k_{r,HW}} = \sqrt{\frac{(1+a/h)}{b_*(1-a/h)}}\left[\frac{\sqrt{\left(\Lambda_e - b_*(1-a/h)\right)^2+\left(\frac{\Lambda_e r_*}{b_*(1-a/h)}\right)^2}+\Lambda_e - b_*(1-a/h)}{\sqrt{\left(\Lambda_e-(1+a/h)\right)^2+\left(\frac{\Lambda_e r_*}{(1+a/h)}\right)^2}+\Lambda_e-(1+a/h)}\right]^{1/2} \tag{6}$$

in which we have defined the dimensionless complex wave number κ, the dimensionless friction parameter r_* and the estuarine convergence number Λ_e:

$$\begin{aligned}
&\kappa = \kappa_r + i\kappa_i = 2kL_b \\
&L_* = \frac{2L_b\omega}{\sqrt{gh}} = \frac{2L_b}{L_g}, \quad \text{where} \quad L_g \equiv \frac{\sqrt{gh}}{\omega} \\
&r_* = \frac{r}{\omega h} = \frac{gU}{\omega h C^2} = \frac{L_t}{L_f}, \quad \text{where} \quad L_f \equiv \frac{hC^2}{g} \text{ and } \quad L_t \equiv \frac{U}{\omega} \\
&b_* = \frac{b_c+\Delta b}{b_c} \\
&\Lambda_e = b_* L_*^2 = \frac{b_c+\Delta b}{b_c}\frac{4L_b^2\omega^2}{gh} = \left(\frac{2L_b}{L_{g,cp}}\right)^2, \quad \text{where} \quad L_{g,cp} \equiv \frac{\sqrt{gA_c/b_{tot}}}{\omega}
\end{aligned} \tag{7}$$

The dispersion equation (A.3) appears to be governed by five length scales, i.e. the convergence length L_b, the tidal length scale in a rectangular and compound channel L_g and $L_{g,cp}$, the tidal excursion L_t, and the friction length L_f. Also, we introduce the estuarine convergence number Λ_e, through which all geometrical and bathymetrical features of the rivers are accounted for. Λ_e decreases with increasing water depth and river convergence, and with loss of intertidal area.

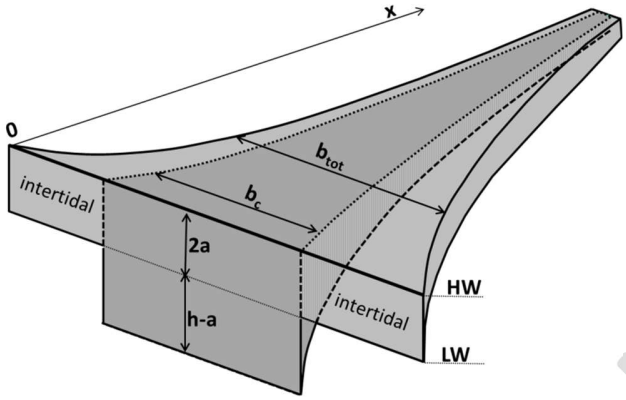

Fig. 4: Schematic estuary for linear analysis.

The behavior of equ. (5) and (6) at a station 40 km up-estuary in a narrow, sandy infinitely long tidal river with convergence length L_b = 30 km and Chézy coefficient C = 60 m$^{1/2}$/s is shown in Fig. 5 and 6 as a function of water depth for four values of intertidal area ($\Delta b/b_c$ = 0; 0.1; 0.2 and 1). The tidal amplitude at the mouth a_0 is set at 0.5 m, so that the characteristic velocity U amounts to about 0.6 – 0.7 m/s. Fig. 5a presents the amplification factor a/a_0 as a function of the estuarine convergence number Λ_e, i.e. equ. (5). Note that these lines do not collapse, as the friction parameter r_* is a function of h, which also affects Λ_e. In the range of $0.5 < \Lambda_e < 4$, a/a_0 reduces rapidly, whereas the results for $\Delta b/b_c$ = 0; 0.1; 0.2 almost collapse. Only for larger intertidal areas, the results start to deviate. Fig. 5b presents the amplification factor a/a_0 as a function of water depth, showing a rapid increase up to about h = 8 – 10 m. For the present settings, the tide becomes amplified $(a/a_0 > 1)$ at x = 40 km for water depth beyond h = 7 m. Amplification is a bit retarded with increasing intertidal, though a/a_0 at larger water depth becomes larger than without intertidal as a result of the larger water storage. The deviating behavior for larger intertidal can be understood by realizing that the celerity is a function of the river's hypsometry $\left(c = \sqrt{gV_c/b_{tot}}\right)$, which affects the resonance characteristics of the tide in the river (Dronkers, 1964).

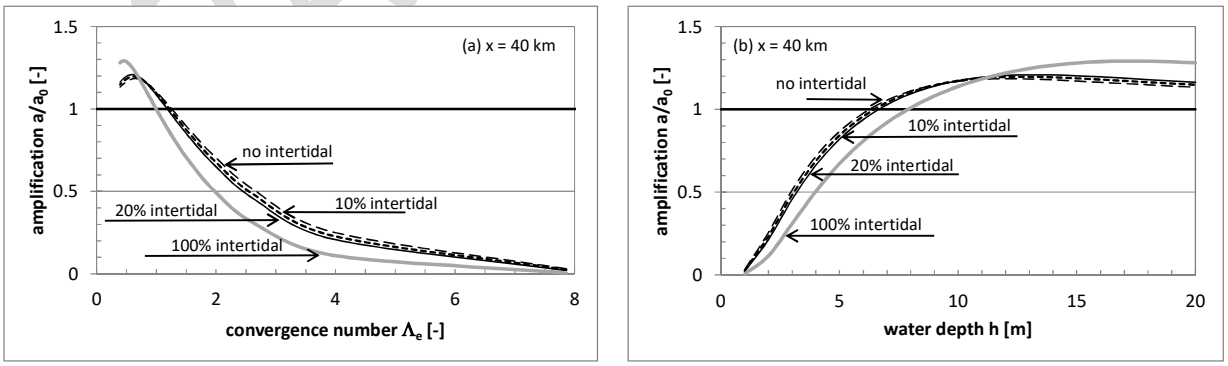

Fig. 5: Tidal amplification for four values of intertidal area as a function of (a) the estuarine convergence number and (b) water depth.

The tidal asymmetry parameter γ_e as a function of Λ_e and h is presented in Fig. 6a and 6b, respectively, showing that without intertidal area, conditions are always flood-dominant ($\gamma_c > 1$), whereas for large intertidal area, conditions are always ebb-dominant, consistent with the summary in the introduction. Further, the results show that for $h < 4 – 5$ m, γ_e first increases with increasing h, while at larger depth, γ_e decreases with h. This is consistent with our arguments in the introduction that changes in residual transport in response to deepening a fairway are determined by a competition between an increase by tidal amplification, and a reduction by tidal asymmetry.

This analysis shows that for the present parameters, conditions are always ebb-dominant for intertidal areas with $\Delta b/b_c > 1.2$. Tidal rivers with small intertidal $\Delta b/b_c \approx 1.1$ exhibit irregular behavior, with ebb- or flood-dominant conditions depending on water depth, further to the role of hypsometry.

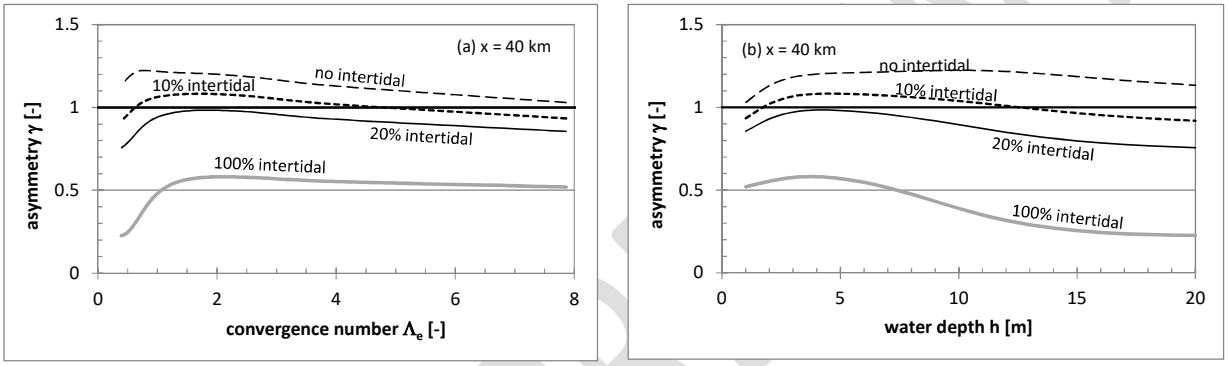

Fig. 6: Tidal asymmetry parameter for three values of intertidal area (as percentage of the flow-carrying area) as a function of (a) the estuarine convergence number and (b) water depth.

This irregular behavior is further exemplified in Fig. 7, showing the longitudinal variation of tidal amplification and asymmetry for $\Delta b/b_c = 1.1$ for three water depth, i.e. h = 5; 10; and 15 m. For h = 5 and

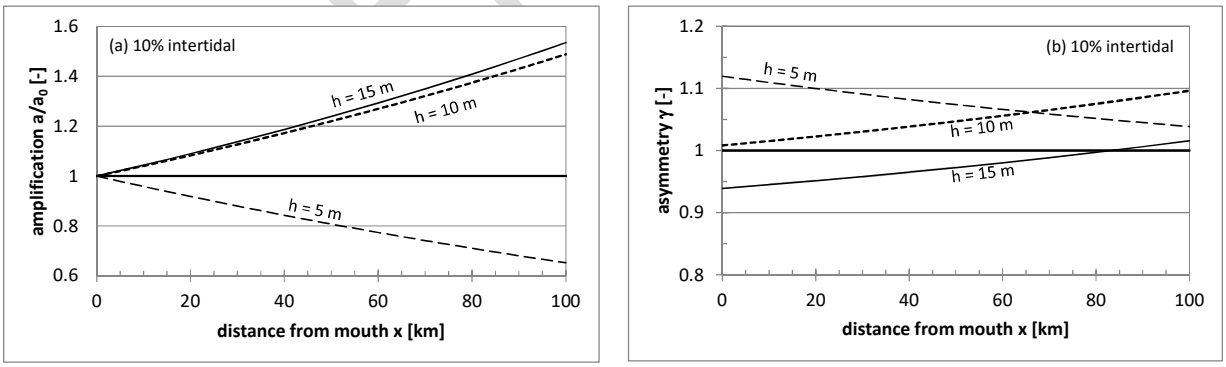

Fig. 7: Longitudinal variation of tidal amplification and asymmetry for small intertidal area at three water depths.

10 m, the river is flood-dominant over its first 100 km, whereas for h = 15 m, conditions are ebb-dominant over the first 80 km, while beyond the river becomes flood-dominant. Further, for h = 5 m, the tide is damped, reducing the tidal amplitude up-estuary. At $h \approx 7$ m, the amplification factor becomes unity (i.e. constant tidal range along the river), and beyond, the tide becomes amplified, resulting in an increasing

tidal asymmetry up-estuary. For the present settings with horizontal bed, the larger tidal asymmetry is found at the head of the estuary.

The findings above are further elaborated in the form of the ebb-/flood-dominance transition in residual sediment transport of Fig. 3 for various convergence lengths (L_b = 20, 30 and 40 km), and various roughness coefficients (C = 40, 60 and 80 m$^{1/2}$/s, i.e. rough, median, smooth). The characteristic velocity U in the friction parameter r_* is obtained from the zero-order approximation $U = a\sqrt{gh}/h$. The results at x = 100 km in the prismatic, rectangular channel (Fig. 4) are given in Fig. 8. Above the transition lines, conditions are fully ebb-dominant over the entire 100 km. Below these lines, at least part of the tidal river is characterized by flood-dominant conditions. As the tidal amplitude is amplified or damped, a/h varies along the river, as a result of which one part of the river is ebb-dominant, while another part is flood-dominant with respect to the residual sediment transport. Only for very small intertidal area of large values of a_0/h, the entire river becomes flood dominant.

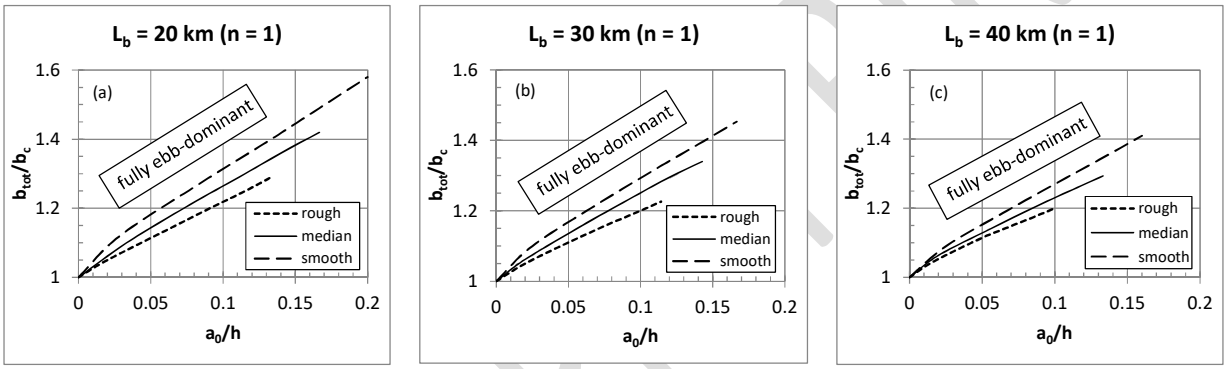

Fig. 8: Effect convergence length L_b and roughness at x = 100 km on residual sediment transport by tidal asymmetry (rough: C = 40 m$^{1/2}$/s; median: C = 60 m$^{1/2}$/s; smooth: C = 80 m$^{1/2}$/s).

This analysis shows that even in a regularly shaped tidal river, the local residual sediment transport may exhibit irregular behavior. Real tidal rivers are much less regular, even when engineered heavily. Their hypsometry, depth and intertidal area often vary considerably along their length, and sometimes over seasons as well (e.g. high river flow flood plains). To assess the overall response of a tidal river to deepening, another, integrating step has to be made.

Tidal asymmetry, residual sediment transport and morphology

In the previous sections, the response of the residual sediment transport to deepening is elaborated as a function of tidal asymmetry, accounting for the local hypsometry of the tidal river. However, the morphodynamic response of the entire river to deepening is governed by the integrated effect of changes in residual sediment transport, and their gradients, which in turn affect the tidal asymmetry, etc. This induces the morphodynamic response cycle in Fig. 9. We have distinguished between asymmetry in the vertical tide and in the horizontal tide, further to the analyses of the literature in the first part of this paper. However, these asymmetries are two sides of the same coin: they are inseparable connected through the continuity of water, as indicated by the box in Fig. 9. This explains also why the analysis by Friedrichs

and Aubrey (1988) and Dronkers (1986) are so similar, though the first focused primarily on the vertical tide in their analysis, whereas Dronker (1986) combined the two asymmetries.

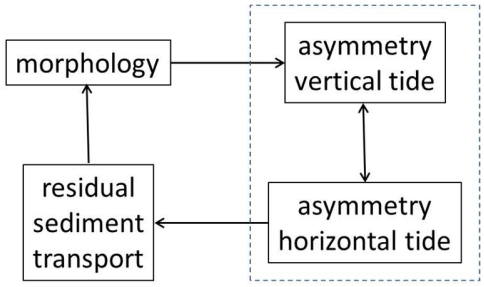

Fig. 9: Morphodynamic cycle relating tidal asymmetry, residual sediment transport and river response to deepening.

Fig. 10 sketches the deformation of an initially sinusoidal progressive tidal wave in response to the larger celerity at HW than at LW, as in Dronkers (1986) approach. In an Eulerian frame of reference, this implies that the period of falling water exceeds that of rising water (largely). As tidal velocities scale with $\mathrm{d}h/\mathrm{d}t$, tidal velocities are large at the beginning of the rising tide,.

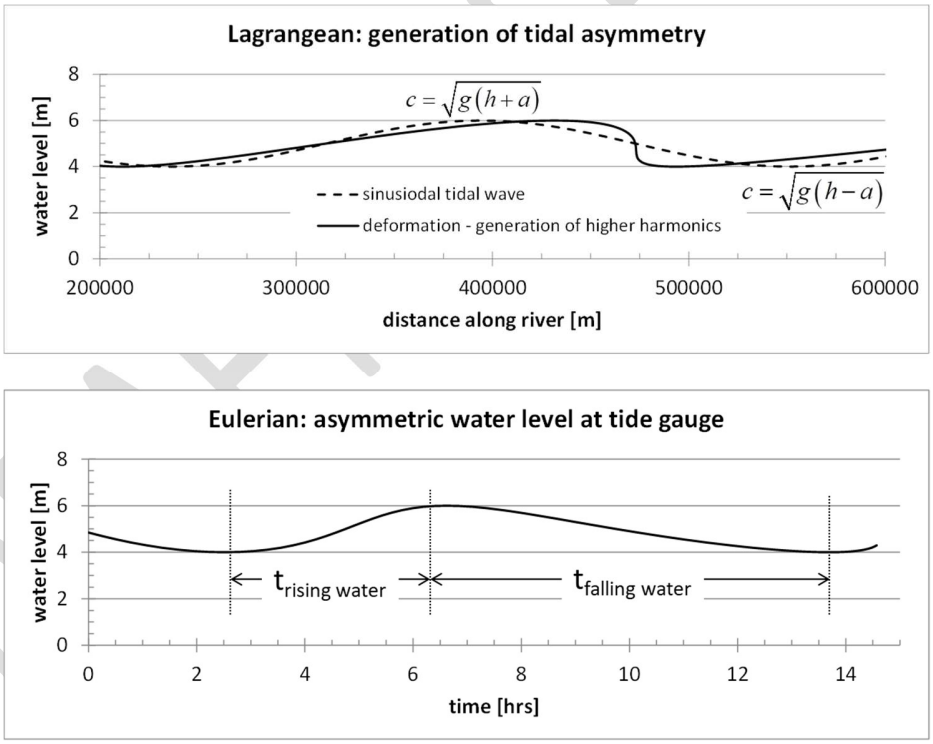

Fig. 10: Deformation of the progressive tidal wave in a Lagrangian and Eulerian frame of reference.

This is visualized in Fig. 11, showing the measured vertical and horizontal tide in the Ems River, close to Leerort (Wang, 2010), illustrating the large asymmetry in tidal velocity, with peak flood velocities about 50% higher than the peak ebb velocities, and the rapid increase in flood velocity after low water slack (LWS). Fig. 11 also shows the shorter period of rising water compared to that of falling water. Hence, as

discussed by Wang et al. (1999), the asymmetries in vertical and horizontal tide are inseparably connected.

Thus, further to equ. (2), tidal asymmetry at any location x along the river can be identified from T_{HW} and T_{LW}, the travel times of HW and LW (more accurately of the tide's crest and trough), respectively:

$$T_{HW}(x) = \int_{x_m}^{x} \frac{\mathrm{d}x'}{c_{HW}} \quad \text{and} \quad T_{LW}(x) = \int_{x_m}^{x} \frac{\mathrm{d}x'}{c_{LW}} \tag{8}$$

with $x = x_m$ at the river mouth (see also discussion section). Thus flood-dominant conditions at location x are expected when $T_{HW} < T_{LW}$, and vice versa. This implies that it is not the local γ_c that determines flood-/ebb-dominance, but its along-river integration. Thus small variations in γ_c along the river, owing to irregularities in the hypsometry of a tidal river with an otherwise fairly regular cross section distribution will not affect the overall asymmetry, thus residual sediment transport and river's morphlogy. In that case, the local asymmetry parameter γ_c can be used to analyze the overall river behavior, provided a characteristic value is used. The previous section shows, however, that even in completely prismatic rivers, the local γ_c may deviate from its overall characteristic value. This is even more the case in natural and engineered rivers where the hypsometry may vary substantially along the river, with larger and smaller intertidal areas, variations in the shape and size of the cross section, etc. It is therefore important to choose locations for the assessment of γ_c wisely.

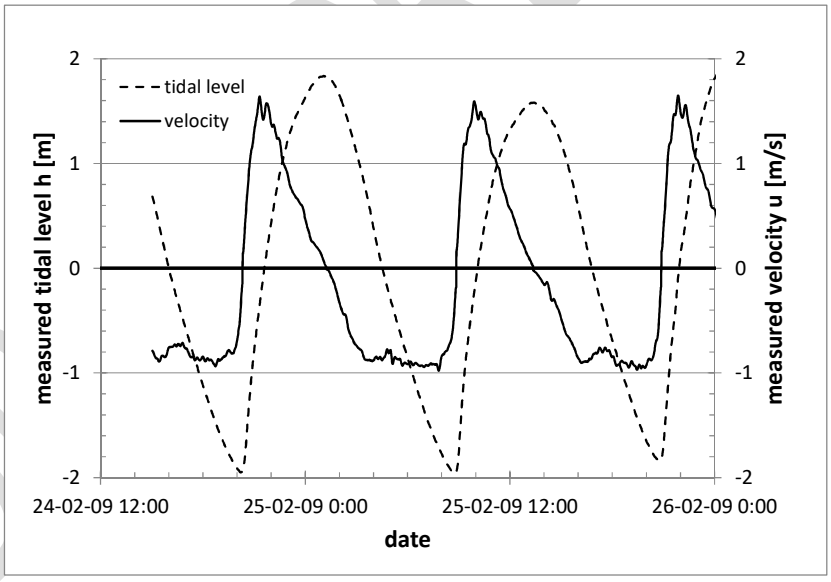

Fig. 11: Vertical and horizontal tide measured in the Ems River (courtesy, Wang, 2010).

The relation between vertical and horizontal tide can be further understood from the continuity equation in a tidal river with the hypsometry of Fig. 4, formalizing the mass balance between two cross sections at $x = x_1$ and $x = x_2$:

$$A_c(x_1)u(x_1) - A_c(x_2)u(x_2) = \int_{x_1}^{x_2} (b_c + \Delta b)\frac{\partial \eta}{\partial t}\,\mathrm{d}x' \tag{9}$$

where η = local water level. If x_2 would be situated well up-estuary, where tidal velocities would vanish, equ. (9) becomes:

$$A_c(x)u(x) = \int_{x}^{\infty} (b_c + \Delta b)\frac{\partial \eta}{\partial t}\,\mathrm{d}x' \tag{10}$$

Equ. (10) implies that the (tidal) discharge through any cross section in the river is governed by the tidal water level variations in the entire river stretch up-river from that cross section. This argument also holds for the distribution of the discharge, thus its asymmetry, implying that the residual sediment transport in a tidal river should be integrated over the entire river, consistent with our argument on high and low water propagation times.

It is noted that in general, water level and flow velocity in a tidal river are not in phase. This implies that asymmetries in discharge $(Q \propto h \times u)$ and in u are not identical: it is rare that peak flood discharges are larger than peak ebb values, whereas in many cases peak flood velocities are larger than peak ebb velocities.

Discussion and conclusions

This paper describes conceptually the response of a narrow, relatively long sandy tidal river to anthropogenic deepening, with focus on the role of tidal asymmetry and amplification. We have argued that the different travel times of the high and low water wave in a tidal river induce tidal deformation, and yield a good parameterization of the asymmetries in the horizontal tide (the tidal velocities), i.e. in the peak ebb and peak flood velocities. These asymmetries steer the residual sediment transport in the river, thus governing its morphodynamic response to deepening. In case of a fairly regular longitudinal distribution of the river's hypsometry, the local tidal asymmetry parameter γ_c, as proposed in literature, provides a useful proxy of the overall asymmetry in the river. However, this local parameter depends on the local hypsometry only, and a river-wide characteristic value has therefore to be established with care, possibly at a variety of locations. In the case of short basins, the vertical and horizontal tide co-oscillate, and asymmetries in local residual transport may be analyzed in terms of the deformation of the vertical tide only.

The actual residual sediment transport, however, is not only a function of these asymmetries, but also of the absolute magnitude of the tidal flow velocities. A linear analysis shows that even for very schematic cases, the competition between changes in tidal deformation and in tidal amplification may alter both the direction and magnitude of the net response to deepening. It is expected that natural and engineered rivers, with less regular planforms and cross sections, will exhibit an even more irregular response. It is therefore mandatory to relate tidal asymmetry and amplification to a reference station, generally the mouth of the river, where the tide is not (yet) affected by deepening. However, there are a number of other elements

affecting the tidal asymmetry in estuaries, which have not been discussed in the preceding, but may be important. For instance, observations reveal that the tide in the mouth of many rivers is not symmetrical, but already deformed in the shallow surrounding waters where the river debouches. Often, these deformations are prescribed as boundary conditions to the tidal river, enhancing the deformations within the river itself in a non-linear way. This implies that for instance the M4-component in a tidal river cannot be treated as the sum of the external component, prescribed at the river's mouth, and the M4-component generated within the river: this sum would depend on the location of the river mouth (i.e. x_m). Indeed, numerical experiments show that tidal characteristics obtained from simulations with an M4-component prescribed at the river's mouth are quite different from the results of a simulation in which the "external" M4 tide is linearly added to the computational results of a simulation without such an M4-component. Owing to the non-linear interaction between the various tidal components this difference increases with tidal range.

However, the effects of an "external" deformation of the tide can be accounted for if the tidal river is treated as a sub-domain of a larger tidal system, with a symmetrical tide at its boundary, where $x = x_0 = 0$, see equ. (8). The deformation of the tide between x_0 and x_m is also reflected by different travel times of the high and low water wave, thus can be quantified in terms of the difference between flood and ebb tide duration, as in Dronkers' equ. (2). This duration difference is then the starting value at the mouth for assessing the arrival time of LW within the river, whereas the starting value for HW would remain unaltered. The difference between the arrival times of LW and HW is then again a good indicator for the asymmetry of the vertical tide.

In the previous it is implicitly assumed that the river is deepened over its entire length, or at least over a major part. In case of local deepening, as in the case of e.g. sand mining, net sediment transport to re-establish morphodynamic equilibrium, may occur against the direction of tidal asymmetry. Quantification of this re-establishment requires the use of a morphodynamic model.

The analysis of tidal asymmetry above ignores the effect of river flows. However, fresh water river input has five important effects on the net sediment transport in tidal rivers: 1) it induces a residual flow velocity, 2) it affects the tidal propagation itself, 3) it affects low, mean and high water levels, 4) it affects the tidal asymmetry, and 5) it induces gravitational circulation, as elaborated below.

1. Residual flow velocity. A direct effect of the river flow with discharge Q_r is a residual flow velocity u_0 $\left(=Q_r/A_c\right)$, which has direct influence on the net sediment transport (Van de Kreeke and Robaczewska, 1993; Chu et al., 2015). If u_0 is relatively small with respect to the amplitude of M2 velocity u_2, the contribution of the river flow to the net transport of coarse sediment can be calculated from its interaction with the M2 tide (Van de Kreeke and Robaczewska, 1993). Otherwise the interaction between the river flow and all other tidal components needs to be considered to assess the net sediment transport (Chu et al., 2015). Owing to the larger river cross section down-river, the effects of river flow decrease in downstream direction.
2. Tidal propagation and amplification as function of river flow. The river flow reduces tidal amplification (thus damping) by increasing the hydraulic resistance to the flow (Godin, 1991, 1999; Kukulka and Jay, 2003; Moftakhari et al., 2013). This follows from substituting the

combined flow velocity $u_0 + u_2 + ...$ into the quadratic resistance term of the momentum equation. This restricts landwards tidal intrusion along the river.

3. Next to this primary effect, river flow can also increase the mean water depth, reducing the effective hydraulic drag, thus favoring landwards intrusion of the tide. This is effect was quantified by e.g. Jay et al. 2010 in an analysis of the water levels in the Columbia River as a function of river flow Q_{riv}. From a regression analysis they found $h_{MSL} = \mathrm{F}\left\{Q_{riv}^{2/3}, a_0^2 / Q_{riv}^{4/3}\right\}$, and similar relations for the high and low water levels. At larger river flows, the effect is considerable, and linear analyses fail.
4. Tidal asymmetry and river flow. River flow also influences the deformation of the tidal wave propagating up-river (i.e. against the river flow direction). Due to its opposite effects on hydraulic drag during ebb (increase) and flood (decrease), the tidal wave is extra deformed in flood direction (Godin and Martinez, 1994; Guo et al., 2015, 2019). Moreover, the transition between ebb- and flood-dominant transport migrates down-river with increasing river flow (Winterwerp et al., 2017). Wang et al. (2019) analyzed the ratio rising-tide period and falling-tide period T_{rt}/T_{ft} as a function of river flow in the Upper Sea Scheldt and found variations of that ration between 0.65 and 0.3 for river flows varying between 0 and 250 m^3/s. Then T_{rt}/T_{ft} is no longer a measure for tidal asymmetry.
5. Gravitational circulation and river flow. Gravitational circulation is induced by horizontal gradients in water density, e.g. salinity, inducing an up-river near-bed residual velocity component. In case of vertically well-mixed conditions, these near-bed flow velocities are small, and their effect on sand transport is small as well. However, under stratified conditions, the effects can become substantial, with near-bed flow velocities increasing by various dm/s see e.g. Burchard and Baumert, 1998; Geyer and MacCready, 2014). Stratification increases with river flow, but on the other hand, salinity intrusion itself reduces with river flow (Savenije, 2005).

Deepening increases the river cross section, hence the role of river flow on the tidal properties decreases with deepening (effects 1 – 4). However, the effects of gravitational circulation increase (5). First, salinity intrudes further into the river. Secondly, near-bed velocities scale with h^3, hence can increase rapidly with deepening. This implies that for larger river flows, assessment of the response of tidal asymmetry to deepening should be based on an analysis of changes in tidal velocities, as the vertical tide no longer tells the entire story.

In this paper we have summarized in a conceptual way the impact of deepening of a tidal river on tidal propagation, amplification and asymmetry, residual sediment transport and morphology. The response of the (entire) river is governed by a competition between various processes:

1. Deepening reduces tidal asymmetry and enhances tidal amplification (up to a certain water depth),
2. Deepening reduces the effects of river flow on tidal asymmetry, and
3. Deepening enhances salinity intrusion and gravitational circulation.

Because of these non-linear interactions, we believe that in general the response of a tidal river to anthropogenic deepening needs to be evaluated with the use of numerical simulations, accounting for the various processes discussed in this paper, and their interaction/competition. Behavioral models may miss one or more of the interactions/competitions.

This paper deals with coarse, sandy sediment only. However, many rivers contain larger or smaller amounts of fine sediment as well, cohesive or not. Particularly in the latter case, asymmetries in the period of slack water become important, e.g. Winterwerp et al. (2021).

Data availability

The graphs in this manuscript contain graphical representations of the various formulae derived, no field or laboratory data have been used.

References

Burchard, H., Baumert, H., 1998. The formation of estuarine turbidity maxima due to density effects in the salt wedge, a hydrodynamic process study. J. Phys. Oceanogr. 28, 309-321.

De Vet, P. L. M., van Prooijen, B. C., & Wang, Z. B. (2017). The differences in morphological development between the intertidal flats of the Eastern andWestern Scheldt. Geomorphology, 281, 31–42. https://doi.org/10.1016/j.geomorph.2016.12.031

Dronkers JJ (1964) Tidal computations in river and coastal waters. Elsevier, New York

Dronkers, J., 1986. Tidal asymmetry and estuarine morphology. Netherlands Journal of Sea Research 20: 117–131.

Dronkers J (2005) Dynamics of coastal systems. Advanced Series on Ocean Engineering—Vol 25.World Scientific

Friedrichs CT, Aubrey DG (1988) Non-linear tidal distortion in shallow well-mixed estuaries: a synthesis. Estuarine, Coastal and Shelf Science 27(5):521-545

Friedrichs, C. T., and D. G. Aubrey, 1994. Tidal propagation in strongly convergent channels, Journal of Geophysical Research, 99: 3321-3336.

Geyer, W. R., & MacCready, P. (2014). The estuarine circulation. Annual Review of Fluid Mechanics, 46(1), 175–197. https://doi.org/10.1146/annurev-fluid-010313-141302

Godin G 1991, Frictional effects in river tides, in Progress in Tidal Hydrodynamics, edited by B.B. Parker, John Wiley New York.

Godin G (1999) The propagation of tides up rivers with special considerations on the upper Saint Lawrence River. Estuar Coast Shelf Sci 48:307–324.

Godin G., Martinez A., 1994. Numerical experiment to investigate the effect of quadratic friction on the propagation of tides in a channel. Continental Shelf Research 14, 723-748.

Guo L.C., van der Wegen M., Jay D.A., Matte P., Wang Z.B., Roelvink J.A., He Q., 2015. River-tide dynamics: exploration of nonstationary and nonlinear tidal behavior in the Yangtze River estuary. Journal of Geophysical Research: Oceans 120, doi:10.1002/2014JC010491.

Guo, L., Wang, Z. B., Townend, I., & He, Q. (2019). Quantification of tidal asymmetry and its nonstationary variations. Journal of Geophysical Research: Oceans, 124, 773–787. https:// doi.org/10.1029/2018JC014372

Jay, D. A., 1991. Green law revisited: Tidal long-wave propagation in channels with strong topography. Journal of Geophysical Research, 96 (C11) 20,585–20,598.

Jeuken,M., &Wang, Z. (2010). Impact of dredging and dumping on the stability of ebb-flood channel systems. Coastal Engineering, 57(6),553–566. https://doi.org/10.1016/J.COASTALENG.2009.12.004

Kukulka T, Jay DA (2003) Impacts of Columbia River discharge on salmonid habitat: I. A non-stationary fluvial tide model. J. Geophys. Res., 108, 3293.

Lanzoni, S., and G. Seminara, 1998. On tide propagation in convergent estuaries, Journal of Geophysical Research, 103(C13) 30,793–30,812.

Moftakhari HR, Jay DA, Talke SA, Kukulka T, Bromirski PD (2013) A novel approach to flowestimation in tidal rivers,Water Resour. Res., 49, doi:10.1002/wrcr.20363

Parker, B.B., 1991, The relative importance of the various nonlinear mechanisms in a wide range of tidal interactions (review), in Parker B.B. (ed.) Tidal hydrodynamics, J. Wiley & Sons, New York.

Provost, Ch L., 1991, Generation of overtides and compound tides (review), in Parker B.B. (ed.) Tidal hydrodynamics, J. Wiley & Sons, New York.

Savenije, HHG, 2005, Salinity and tides in alluvial estuaries, Gulf Professional Publishing

Speer, P.E. and D. G. Aubrey, 1985. A Study of Non-linear Tidal Propagation in Shallow Inlet/Estuarine Systems - Part II: Theory. Estuarine, Coastal and Shelf Science Vol 21, pp 207-224.

Toffolon, M. and H.G. Savenije, 2011. Revisiting linearized one-dimensional tidal propagation. Journal of Geophysical Research, 116, C07007, doi:10.1029/2010JC006616.

Van Rijn, L.C., 2011. Analytical and numerical analysis of tides and salinities in estuaries; part I: tidal wave propagation in convergent estuaries. Ocean Dynamics, 61: 1719–1741. DOI 10.1007/s10236-011-0453-0.

Wang L (2010) Tide driven dynamics of subaqueous fluid mud layers in turbidity maximum zones of German estuaries. Am Fachbereich Geowissenschaften Der Universität Bremen, PhD-thesis

Wang, Z. B., Juken, H., & de Vriend, H. J. (1999). Tidal asymmetry and residual sediment transport in estuaries. WL|Hydraulic, report No. Z2749, 66 pp.

Winterwerp, J.C. and Z.B. Wang, 2013a, Man-induced regime shifts in small estuaries – I: theory, Ocean Dynamics, Vol 63, pp 1279-1292, DOI 10.1007/s10236-013-0662-9

Wang, Z. B., VanMaren, D. S., Ding, P. X., Yang, S. L., Van Prooijen, B. C., De Vet, P. L.M., et al. (2015). Human impacts onmorphodynamic thresholds in estuarine systems. Continental Shelf Research, 111, CSR3681. https://doi.org/10.1016/j.csr.2015.08.009

Winterwerp JC, Wang ZB, Van Brackel A, Van Holland G, Kösters F (2013b) Man-induced regime shifts in small estuaries—II: a comparison of rivers. Ocean Dyn 63:1293–1306. https://doi.org/10.1007/s10236-013-0663-8

Winterwerp, J.C., J. Vroom, Z.-B. Wang, M. Krebs, H.C.M. Hendriks, D.S. Van Maren, K. Schrottke, C. Borgsmüller and A. Schöl, 2017. "SPM response to variations in hydrodynamics in the Ems River", Ocean Dynamics, Vol 67, pp 559 - 583, DOI 10.1007/s10236-017-1043-6.

Winterwerp, J.C., Van Kessel, T, Van Maren, S.B. and Van Prooijen B.C., 2021. Fine sediment in open water – from fundamentals to modeling. World Scientific, in press.

Appendix A: Derivation of asymmetry parameter γ_e

In this appendix we derive the tidal amplification and asymmetry parameters in an exponentially converging tidal river for the conditions and parameters described in the main text. The governing equations for the conservation of mass and momentum are linearized by neglecting advection and linearizing friction:

$$\begin{aligned} &\left(b_c+\Delta b\right)\frac{\partial \eta}{\partial t}+\frac{\partial A_c u}{\partial x}=0 \\ &\frac{\partial u}{\partial t}+g\frac{\partial \eta}{\partial x}+\frac{ru}{h}=0 \end{aligned} \qquad \text{(A.1)}$$

where η is the instantaneous water level, u is the cross-sectional averaged flow velocity, r is the linear friction term $\left(r=8c_DU/3\pi\ \left[\mathrm{m/s}\right]\right)$, c_D is the drag coefficient, U is a characteristic (maximal velocity), and x and t are longitudinal co-ordinate and time ($x = 0$ at the estuaries mouth, and $x > 0$ up-estuary). The drag coefficient c_D attains values of 0.001 to 0.003 (corresponding Chézy values of 100 – 60 $\mathrm{m^{1/2}/s}$, as $r \approx gU/C^2$). Thus r also varies from around 0.001 to 0.003. The role of fresh water discharge is discussed in the main text, but neglected in the first part of the analysis. Finally, we also assume that the tidal amplitude is much smaller than the water depth and that all parameter variations along the estuary are small. We assume that the solution to (A.1) are given by harmonic functions:

$$\eta\left(x,t\right)=h+a_0\exp\left\{i\left(\omega t-kx\right)\right\} \quad \text{and} \quad u\left(x,t\right)=U_0\exp\left\{i\left(\omega t-kx-\varphi\right)\right\} \qquad \text{(A.2)}$$

where a_0 is the tidal amplitude at $x = 0$, U_0 is the amplitude flow velocity at $x = 0$, ω is the tidal frequency; $\omega = 2\pi/T$; T is the tidal period, k is the complex wave number; $k = k_r + ik_i$, k_r is the real wave number ($k_r = 2\pi/\lambda$), λ is the tidal wave length, k_i is the imaginary wave number, and φ is the phase angle between tide and velocity. Similar configurations were studied by e.g. Jay (1991); Lanzoni and Seminara (1998); Friedrichs and Aubrey (1994); Toffolon and Savenije (2011); and Van Rijn (2011). Substitution of (A.2)

into (A.1) yields a dispersion equation implicit in the wave number k (see Winterwerp and Wang, 2013a for details):

$$L_b k^2 - ik - \frac{b_c + \Delta b}{ghb_c} L_b \omega^2 \left(1 - i\frac{r}{\omega h}\right) = 0 \quad \text{or} \quad \kappa^2 - 2i\kappa - \Lambda_e \left(1 - ir_*\right) = 0 \tag{A.3}$$

in which the dimensionless parameters of equ. (7) have been used. Solving equ. (A.3), gives the real and imaginary wave number, κ_r and κ_i, respectively:

$$\kappa_r = \frac{1}{2}\left[2\sqrt{\left(\Lambda_e - 1\right)^2 + \left(\Lambda_e r_*\right)^2} + 2\left(\Lambda_e - 1\right)\right]^{1/2} \tag{A.4a}$$

and

$$\kappa_i = 1 - \frac{1}{2}\left[2\sqrt{\left(\Lambda_e - 1\right)^2 + \left(\Lambda_e r_*\right)^2} - 2\left(\Lambda_e - 1\right)\right]^{1/2} \tag{A.4b}$$

in which we account for the incoming wave only (no reflections). As tidal amplification/damping varies along the estuary further to $a(x) = a_0 \exp\{k_i x\}$, the relative tidal amplitude along the estuary becomes:

$$\frac{a(x)}{h} = \frac{a_0}{h}\frac{a}{a_0} = \frac{a_0}{h}\exp\left\{\frac{1}{2L_b}\left(1 - \frac{1}{2}\left[2\sqrt{\left(\Lambda_e - 1\right)^2 + \left(\Lambda_e r_*\right)^2} - 2\left(\Lambda_e - 1\right)\right]^{1/2}\right)x\right\} \tag{A.5}$$

This relative amplitude is substituted into the asymmetry parameter γ_c, which thus also varies along the estuary and reads (Winterwerp and Wang, 2013a):

$$\gamma_c(x) = \frac{k_{r,LW}}{k_{r,HW}} = \sqrt{\frac{\left(1 + a/h\right)}{b_*\left(1 - a/h\right)}}\left[\frac{\sqrt{\left(\Lambda_e - b_*\left(1 - a/h\right)\right)^2 + \left(\dfrac{\Lambda_e r_*}{b_*\left(1 - a/h\right)}\right)^2} + \Lambda_e - b_*\left(1 - a/h\right)}{\sqrt{\left(\Lambda_e - \left(1 + a/h\right)\right)^2 + \left(\dfrac{\Lambda_e r_*}{\left(1 + a/h\right)}\right)^2} + \Lambda_e - \left(1 + a/h\right)}\right]^{1/2} \tag{A.6}$$